J Solid State Electrochem (2007) 11:1059–1069
DOI 10.1007/s10008-007-0268-6

ORIGINAL PAPER

Progress in the understanding of tyramine electropolymerisation mechanism

A. M. Tenreiro · C. Nabais · J. P. Correia · F. M. S. S. Fernandes · J. R. Romero · L. M. Abrantes

Received: 5 September 2006 / Revised: 9 October 2006 / Accepted: 11 October 2006 / Published online: 17 February 2007

Abstract The potentiodynamic electrosynthesis of polytyramine (PTy) from acidic medium is analysed on the basis of the information collected by coupling cyclic voltammetry and electrochemical quartz crystal microbalance (EQCM), ellipsometry and atomic force microscopy (AFM). The experimental results consistently indicate that different stages must be considered in a description of the polymerisation process, the first involving the formation of a poor-conducting, thin, smooth and homogeneous layer; at a later stage deposition kinetics change and eventually a nonplanar thick film is produced. A tentative polymerisation mechanism is proposed, which finds support on the ab initio calculations carried out to predict the reactive sites for tyramine (Ty) oxidation and polymer growth.

Keywords Tyramine · Electropolymerisation · Electrooxidation mechanism · ab initio methods

A. M. Tenreiro · C. Nabais · J. P. Correia · L. M. Abrantes (✉)
Centro de Química e Bioquímica,
Faculdade de Ciências da Universidade de Lisboa,
Campo Grande, 1749-016,
Lisboa, Portugal
e-mail: luisa.abrantes@fc.ul.pt

F. M. S. S. Fernandes
Laboratório de Simulação Molecular,
Faculdade de Ciências da Universidade de Lisboa,
Campo Grande, 1749-016,
Lisboa, Portugal

J. R. Romero
Departamento de Química, F.F.C.LR.P.-USP,
Av. Bandeirantes 3400,
14040-910 Ribeirão Preto, São Paolo, Brazil

Introduction

The electropolymerisation of phenol and phenol derivatives has received considerable attention due to their importance in environmental and industrial applications [1, 2]. However, several mechanistic aspects are still unclear due to the complex electrochemistry of the phenol derivatives, which is strongly dependent on the type, position and number of substituents as well as on the chosen experimental conditions [3–6].

It is known [7–9] that the electrooxidation of phenols produces phenoxy radicals, which, reacting with a phenol molecule yield to a para-linked dimmer; further oxidation leads to oligomers and eventually to the formation of a passivating insulating film.

The ability of the electrochemical quartz crystal microbalance, EQCM, in probing the electrode surface modification due to phenol, para-substituted and chlorinated derivatives electropolymerisation, has been illustrated by Wang [10]. The author compared typical time-frequency recordings and respective voltammograms obtained during the oxidation of different phenolic compounds (phenol, 4-chlorophenol, *p*-cresol and 2,4 dichlorophenol) and he observed, for the para-substituted compounds, a single drop in the frequency during the first voltammetric scan concomitant with the disappearance of the voltammetric oxidation peak in subsequent potential scans, while a more gradual deactivation process was recorded for 2,4 dichlorophenol. These results illustrate the influence of the monomer type of substitution on the formation of species other than para-linked ones.

For phenol derivatives with amino groups, the reported voltammetric studies [11] have been interpreted by analogy with the well-established aniline oxidation, i.e. a E(CE)n mechanism; the oxidation of *o*-aminophenol was described

as producing a ladder-structured film and reactive intermediates of 2-amino-phenoxazin-3-1 formation in solution.

In the case of tyramine (4-(2-aminoethyl)phenol (Ty), because the amino function is separated from the phenolic ring by two methylene groups, it is expected that only the phenol moiety is oxidised to perform the polymerisation. However, early studies [12] carried out in methanol-sodium hydroxide solutions have shown that potentiodynamically prepared polymer films displayed a very low conductivity. In acidic aqueous solution, the amino group is protonated and more recent investigations [13] involving Fourier transform infrared spectroscopy (FTIR) and X-ray photoelectron spectroscopy (XPS) spectra analysis support the formation of a polymer with a strong polycationic nature with a structure as given in Scheme 1.

In the present work, results of a detailed study on the electrosynthesis of polytyramine (PTy) are presented. The data obtained by cyclic voltammetry, EQCM, ellipsometry and atomic force microscopy (AFM) provided the basis for a tentative mechanism, which finds support on the ab initio calculations performed to predict the reactive sites for tyramine oxidation and polymer growth.

Materials and methods

Tyramine has been purchased from Sigma and other chemicals, of analytical reagent grade, obtained from Merck. All reagents were used as received and the solutions prepared using Milli-Q water (Millipore).

Electrochemical studies were performed with a Potentiostat CH Instruments model 620A. Experiments were carried out in a three-electrode cell equipped with a Pt disk working electrode (0.196 cm^2 geometrical area), a saturated calomel reference electrode (SCE) and a large platinum foil as counter electrode. Before each electropolymerisation assay, the working electrode was hand-polished in successively finer grades of aqueous suspension of alumina (down to 0.3 μm) until mirror finishing has been generated, followed by consecutive potential cycling, from the hydrogen evolution region to the oxygen evolution domain, −0.45 to +1.40 V vs SCE, in 0.5 mol dm^{-3} H_2SO_4 aqueous solutions. Polytyramine films were potentiodynamically grown from 0.025 mol dm^{-3} Ty in 0.1 mol dm^{-3} H_2SO_4 aqueous solution. All solutions were carefully de-oxygenated by nitrogen bubbling for at least 15 min.

EQCM experiments were performed with a frequency analyzer (CH Instruments model 420), in a single-compartment cell. AT-Cut quartz crystals of 8 MHz fundamental frequency, both sides coated by Pt, were used as working electrodes. A Pt wire and a SCE were used as counter and reference, respectively. The resonant frequency changes were converted into mass variation using the Sauerbrey equation [14]. For crystals used in the present work, a frequency shift of 1 Hz is equivalent to a mass change of 1.39 ng.

The ellipsometric data have been collected with a SENTECH SE 400 ellipsometer, working with a He-Ne laser (λ=632.8 nm) at 70° incident angle. A home-made two-compartment Teflon cell equipped with two optical windows at 20° from the bottom plane, a "specpure" platinum disk, WE (potential controlled against SCE) and a Pt grid CE were used. After mechanical polishing the WE was flame annealed and cooled under high purity nitrogen flux. The solution was thoroughly deoxygenated directly in the cell with nitrogen bubbling (purity>99.9997) for 20 min.

The topographic morphology of the PTy films was analysed by atomic force microscopy, using microfabricated silicon cantilevers; all AFM images were recorded ex situ, at room temperature, in tapping mode with a Nanoscope III Multimode from Digital Instruments.

In the computational calculations geometry optimisations were only performed for the ground state of the molecules at a Restricted Hartree Fock, RHF/6-31G(d) level, until a stationary point was found. No additional vibrational frequencies were calculated to evaluate the stability of the optimised structures. The *z*-matrix optimised parameters (bond lengths, bond angles and dihedrals) were used to estimate the properties of the molecules and their corresponding neutral radicals and radical cations. The last were not optimised as it was considered that there is little variation in the bond lengths after removal of an electron from the lone pair of electrons of the O atom and loss of a proton from the ground state of the molecules (the lone pair of electrons are placed in the non-bonding orbital of the oxygen). The radical properties were calculated at a UHF/6-31G(d) level.

The frontier molecular orbital energy and shape have been obtained from the effective atomic charges estimated by the Mulliken population analysis; the unpaired electron spin density distribution was estimated for the neutral radicals and radical cations to assess inside electrooxidation and coupling reaction mechanisms.

All calculations were performed in gas phase and were carried out with Gaussian 98 program [15]. The pictorial representation of the results was obtained with Molekel program [16].

Scheme 1 Structure proposed for polytyramine in [13]

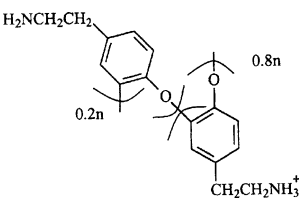

Results and discussion

Figure 1 shows the cyclic voltammetric responses obtained during the potentiodynamic polymerisation of tyramine at 50 mV s^{-1}. Although in the first potential scan, oxidation currents are detectable at about 0.8 V and a well-defined current recorded at 1 V, throughout the reverse potential sweep, the nearby zero current shows no indication of polymer reduction. During the subsequent cycles, a gradual decrease of the anodic current is observed for the first 15 cycles; then the current starts to increase slowly until the 22nd cycle and finally it remains about constant. A similar behaviour has already been reported for PTy electrodeposition performed either from solutions with higher concentration of monomer [17] or carried out by scanning the potential until more anodic potential limits [18].

To help in elucidating the current pattern, the Ty electropolymerisation has been monitored by EQCM as illustrated in Fig. 2. The polymer growth on the electrode surface is clearly demonstrated by the decrease in the frequency, corresponding to a non-regular but continuous mass increase. The data also confirms that the deposited polymer is not reduced within the considered potential domain as the frequency is remarkably constant below 0.8 V, indicating the lack of participation of electrolyte ionic species.

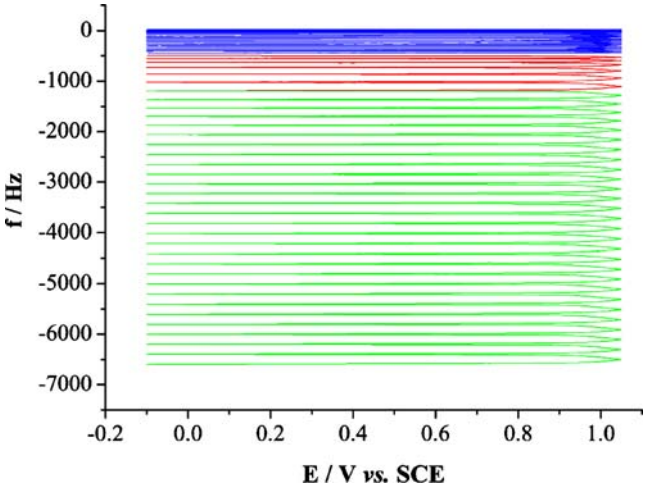

Fig. 2 Resonant frequency changes for the potentiodynamic growth of PTy (same conditions as Fig. 1)

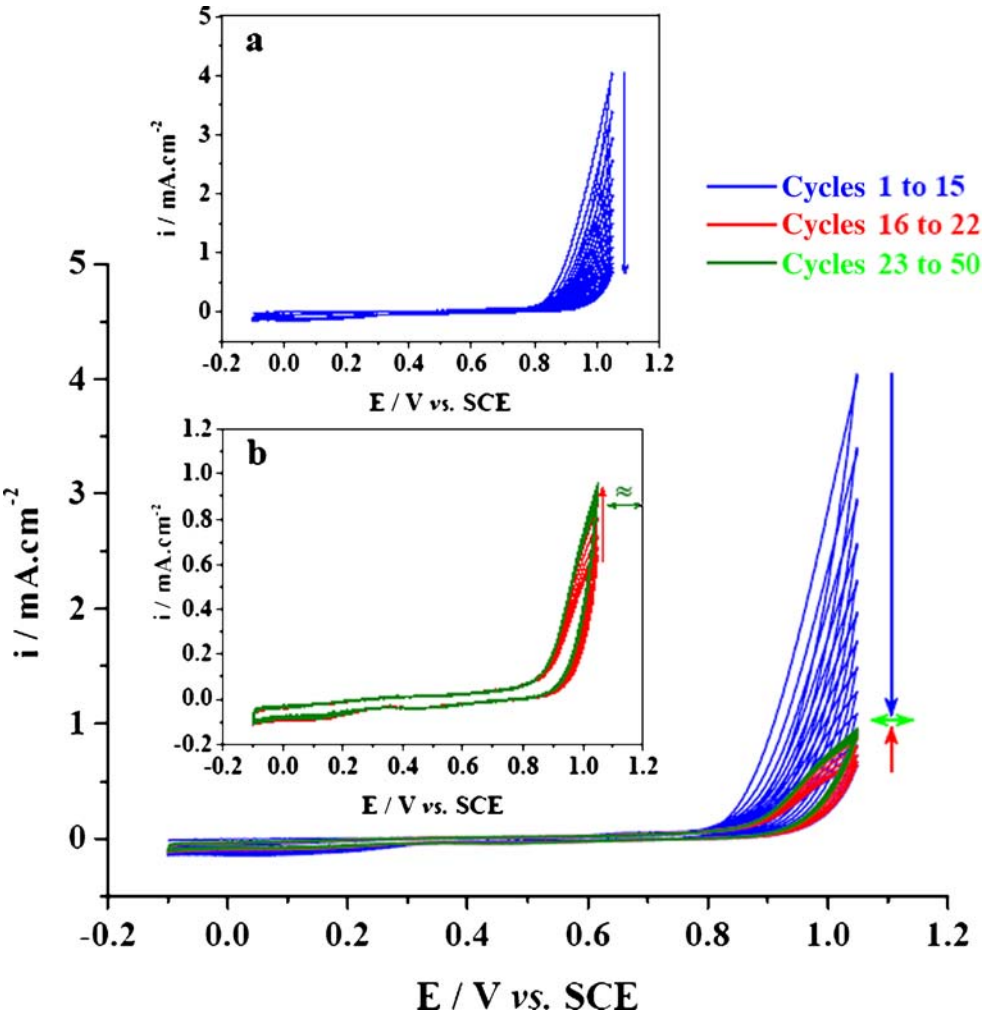

Fig. 1 Cyclic voltammograms for the potentiodynamic growth of PTy (50 cycles from −0.10 to 1.05 V) on Pt electrode from 0.025 mol dm^{-3} Ty in 0.1 mol dm^{-3} H_2SO_4; ν=50 mV s^{-1}; inset **a**: cycles 1st to 15th ; inset **b**: cycles 16th to 50th

Three domains can be identified from the evolution of the frequency change along the process (Fig. 3) pointing to different regimes during the PTy growth. The first corresponds to the very first 15 cycles, where the current was seen to decrease; it might represent the deposition of short and poor-conducting oligomers. The second corresponds to the few following potential cycles where an increase in the current was observed; the much more marked frequency variation strongly suggests that the polymer growth proceeds by another pathway. Finally, it appears that there is an uniform polymer thickening in the region where the current remained nearly constant.

Also shown in Fig. 3 is the relative increase in mass, from cycle to cycle, worked-out using the Saurbrey equation, $\Delta f = -2.26\times10^{-6} f_0^2\ \Delta m$, where Δf represents the changes in resonant frequency of oscillation (Hz), f_0 is the fundamental frequency (Hz) and Δm the changes in mass per unit area (g cm^{-2}). It must be pointed out that the values are merely indicative because a large amount of SO_4^{2-} anions shall be electrostatically associated to protonated amino groups, NH_3^+, and each ion pair is very likely solvated by water molecules. So, the total mass increase depicted in Fig. 4 represents all these contributions and not only the PTy film mass. Notwithstanding, it is interesting to notice that the total increase in mass shows a linear increase with the number of cycles in the first region, in contrast to the period where the anodic current increases, while for further polymer thickening the increase in the whole mass is again linear.

The electrodeposition of PTy on Pt has also been examined by ellipsometry. The changes in the phase shift, $\delta\Delta$, and in the azimuth angle, $\delta\Psi$, measured during the first cycle of the PTy growth are displayed in Fig. 5. It is unequivocally seen by both the sharp modification in $\delta\Delta$ and the inversion in the $\delta\Psi$ signal that the current rise onset corresponds to an alteration in the electrode surface; the surface modification is irreversible as denoted by the optical parameters values during the reverse potential sweep, but there is no indication of deposited material reduction.

As the ellipsometric data have been collected at given potentials for every cycle, (sampling speed of 1 s^{-1}), one can analyse not only the change in the optical parameters, $\delta\Delta$ and $\delta\Psi$, along each potential cycle, but also examine the evolution of the modified electrode optical parameters during the polymer layer thickening, at each potential value. Such analysis, illustrated in Fig. 6, reveals that up to the 15th cycle the decrease in the phase parameter and the increase in the changes of the azimuthal angle are as expected for a polymer layer growth on the electrode surface, while a marked modification in the behaviour is noticed during the following cycles: $\delta\Delta$ increases and $\delta\Psi$ presents very small increments until the 22nd cycle decreasing thereafter, suggesting a non-uniform growth process. During the final cycles the regular changes are again observed.

From the time evolution of the ellipsometric parameters, Δ and Ψ, at different stages of PTy formation (Fig. 7) several important aspects are easily retrieved: (1) there is an early change in the electrode optical parameters (Fig. 7a) indicating that Ty oxidation is easy and processes involving the likely oligomer formation and their precipitation on electrode surface are fast; (2) a difference in the Δ and the Ψ values at the anodic and cathodic potentials limits is observed. Although small for the first 17 cycles, (Fig. 7a) it increases with the number of cycles (Fig. 7b,c) and

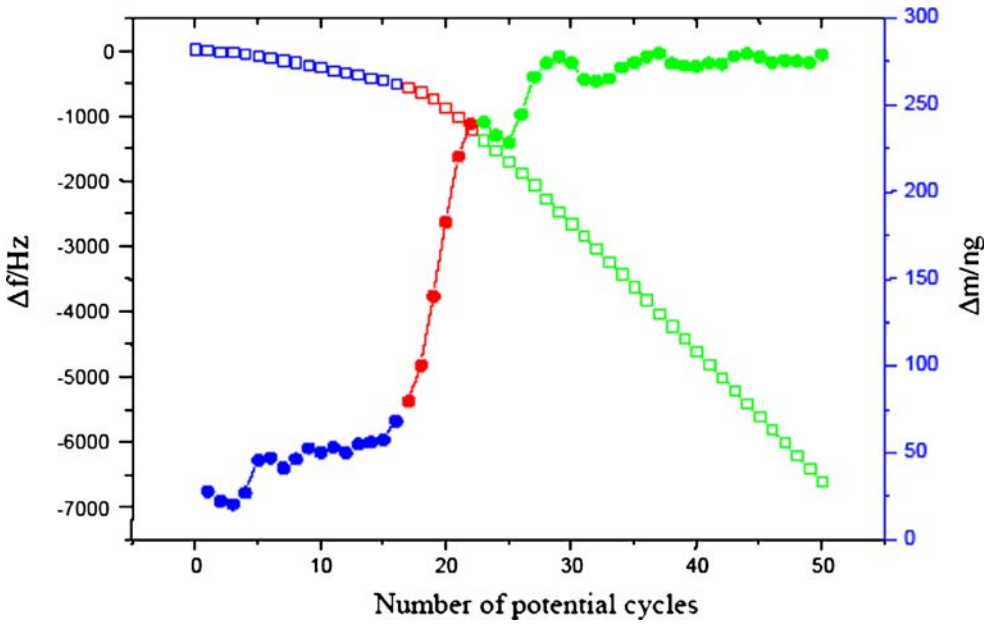

Fig. 3 Relative frequency variation (□) and corresponding mass increase (•) from cycle to cycle, during the potentiodynamic growth of PTy

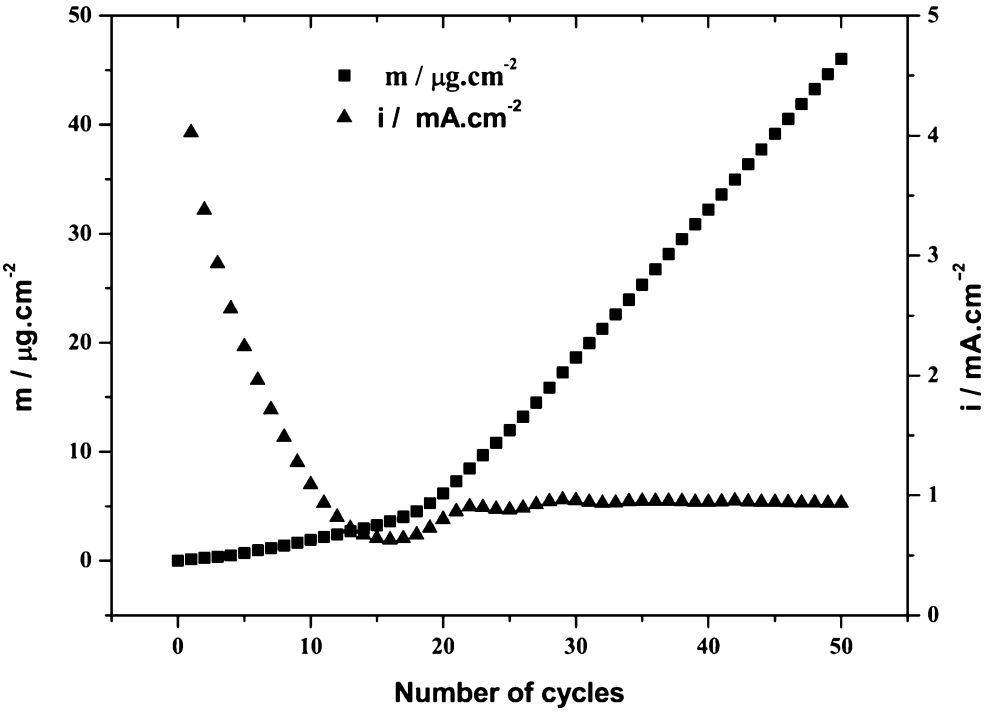

Fig. 4 Total mass increase (▪) during the potentiodynamic polymerisation of PTy. Also shown are the current values (▲) at the anodic potential limit of each consecutive cycle

indicates that the PTy oxidised form does exist in spite of the lack in observing a dedoping process through the cyclic voltammetry or EQCM collected information data; (3) the progressive increase in Ψ reveals the formation of a low absorbing (relatively dense) material; (4) the Δ and Ψ evolution with time for the first region (Fig. 7a) and during the polymer thickening (Fig. 7c) is regular, whereas in the transition region (Fig. 7b) there is an inversion in the evolution of the Δ values.

In an attempt to evaluate the optical properties and thickness of the PTy films being formed, the usual approach of fitting Ψ and Δ values to the three-layer model has been considered for the ellipsometric parameters collected at the anodic potential limit (the procedure is based on finding the complex refractive index that produces Δ vs Ψ theoretical curves, for the homogeneous growth of a layer, with a good fit to the experimental points). As expected, up to about 15 growth cycles, the polymer film is well described by the formation of an homogeneous phase (Fig. 8) with a

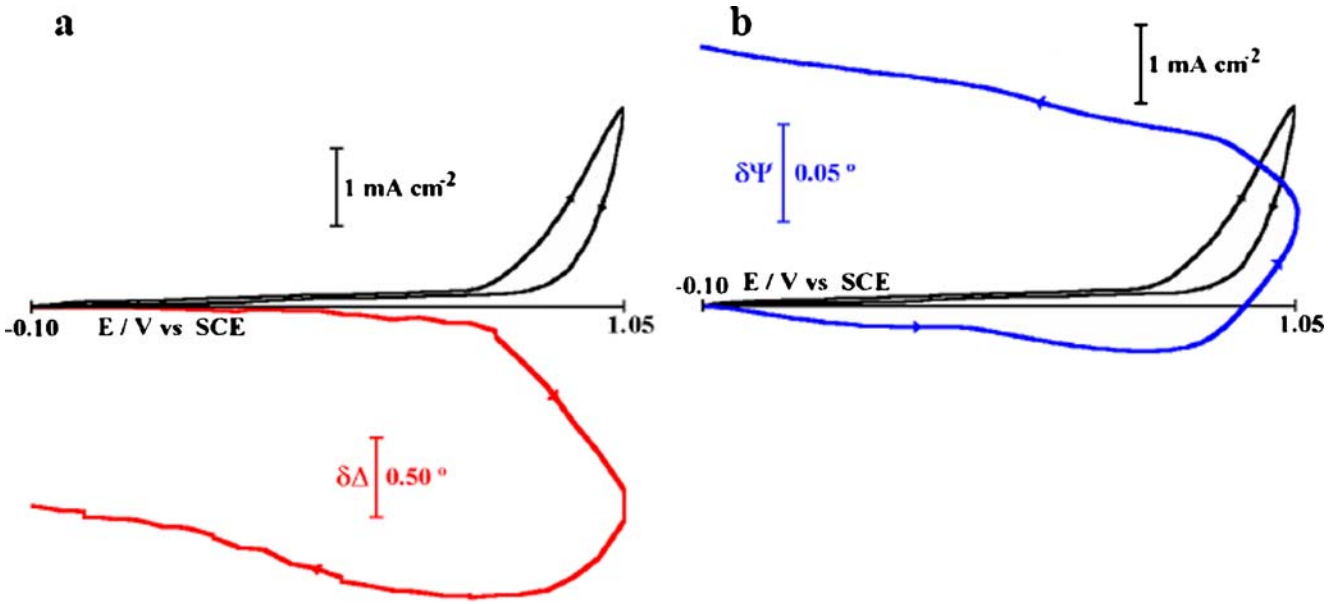

Fig. 5 Changes in the ellipsometric parameters $\delta\Delta$ (**a**) and $\delta\Psi$ (**b**) during the first potential cycle at a Pt electrode in 0.025 mol dm^{-3} Ty in 0.1 mol dm^{-3} H_2SO_4; ν=50 mV s^{-1}. In *black* is also shown the developed current

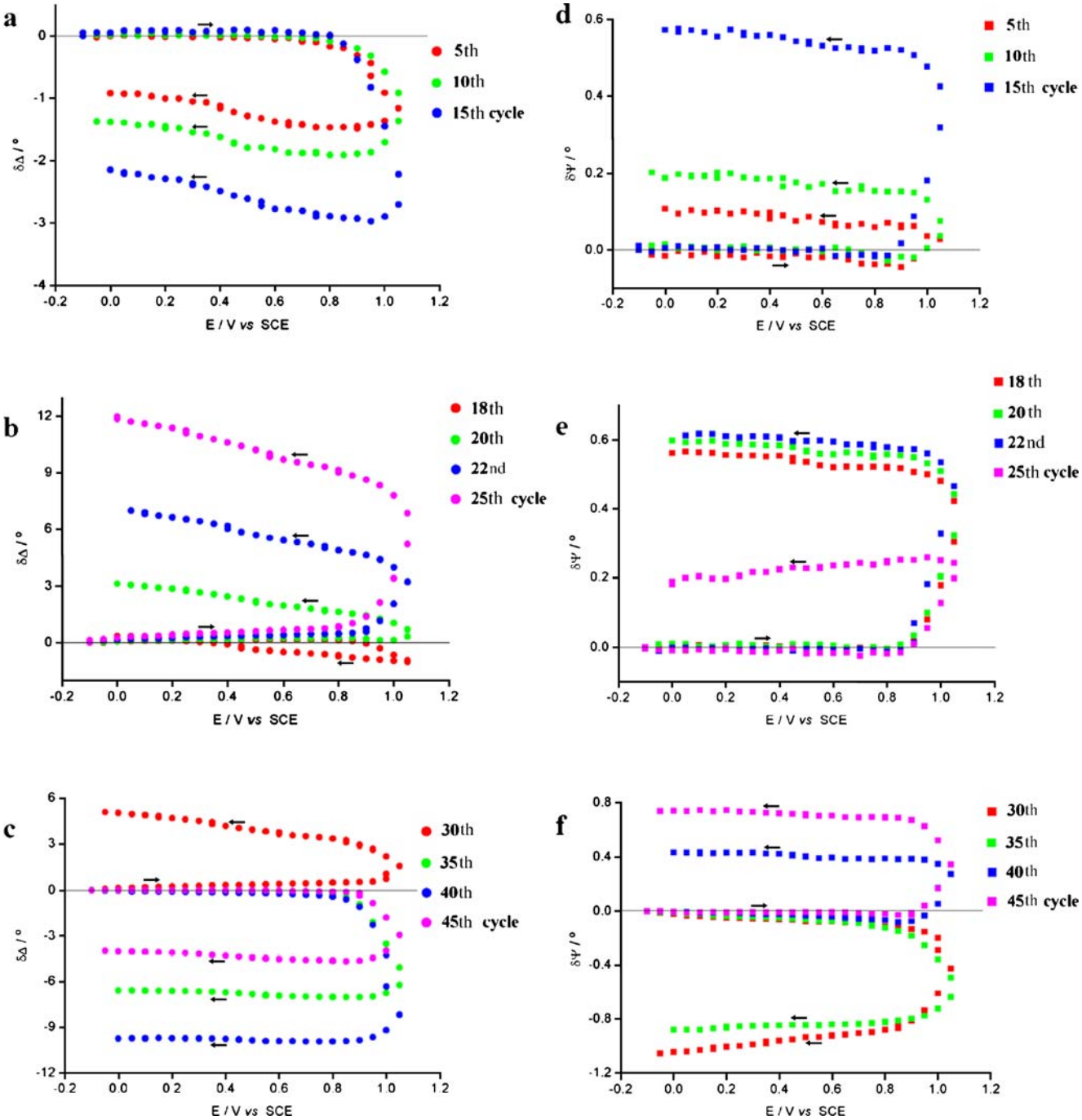

Fig. 6 Changes in $\delta\Delta$ (**a**–**c**) and in $\delta\Psi$ (**d**–**f**) during the thickening of the PTy film

complex refractive index $\tilde{n}$=1.470–0.001i. For the fitting of the subsequent Ψ and Δ values, different theoretical curves are required. The refractive index so obtained for the intermediate layer is probably less exact as it is very likely non-homogeneous and the number of available points are too scarce. However, that evaluation has been considered to allow the fitting of the outer layer; for this, the obtained optical parameters, $\tilde{n}$=1.454–0i indicate the formation of a less dense and transparent material.

The above described procedure also allows estimating the film thickness at the end of each potential cycle. The results, presented in Fig. 9a, reveal a very slow increase during the formation of the first layer in contrast to a rapid out-layer thickness enlargement; combined with the mass increase (Fig. 4), permit information on the film density as displayed in Fig. 9b.

The initial increase in density should be attributed to the progressive formation of a first layer on the electrode

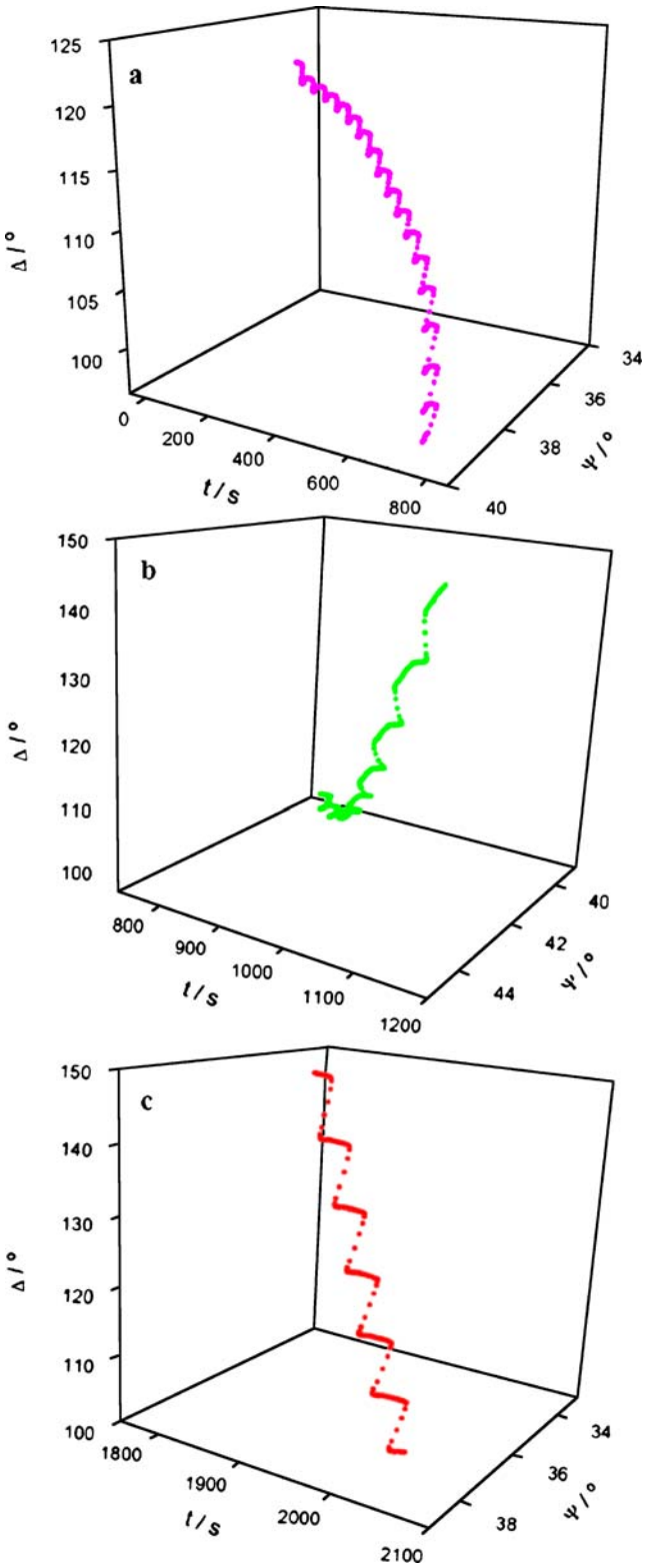

Fig. 7 Time evolution of Δ and Ψ at the different stages of PTy film formation: 1st–17th (**a**) 18th–25th (**b**), and 40th–45th (**c**) potential cycles

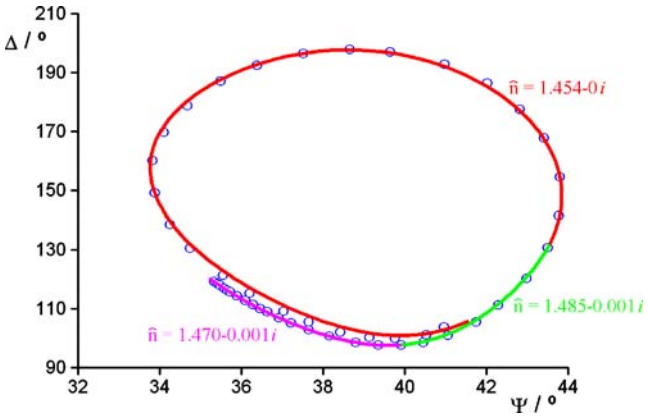

Fig. 8 Fitting of the experimental Ψ and Δ values, collected at the anodic potential limit of the PTy potentiodynamic growth, E=1.05 V, to the three-layer model for the growth of a film on a substrate

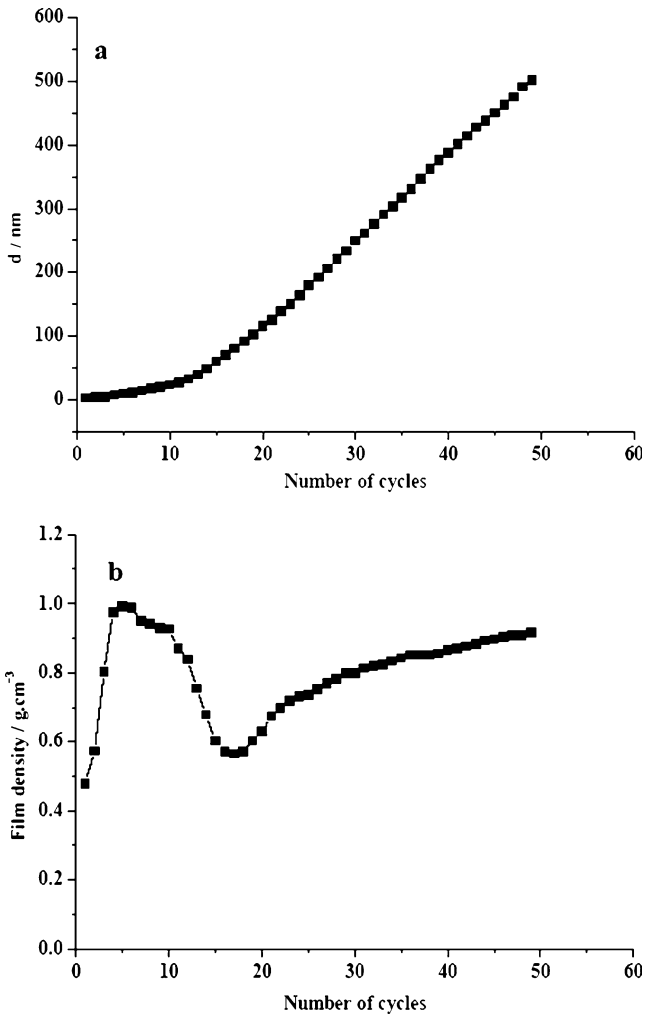

Fig. 9 Dependence on the cycle number of PTy film (**a**) thickness, calculated from the fitting of ellipsometric data collected at the anodic limit at each growth cycle and (**b**) density, calculated from the total mass increase (Fig. 4) and estimated thickness (Fig. 9a)

surface; such layer appears to thicken with about constant density (0.93 g cm^{-3}), but suddenly a deep decrease in density (down to 0.57 g cm^{-3}) is observed pointing to strong conformational modifications responsible to marked volume expansion without equivalent mass input. Particularly interesting is the density increase and the final tendency to a plateau (at about 0.90 g cm^{-3}) as the polymerisation proceeds. A plausible explanation for this

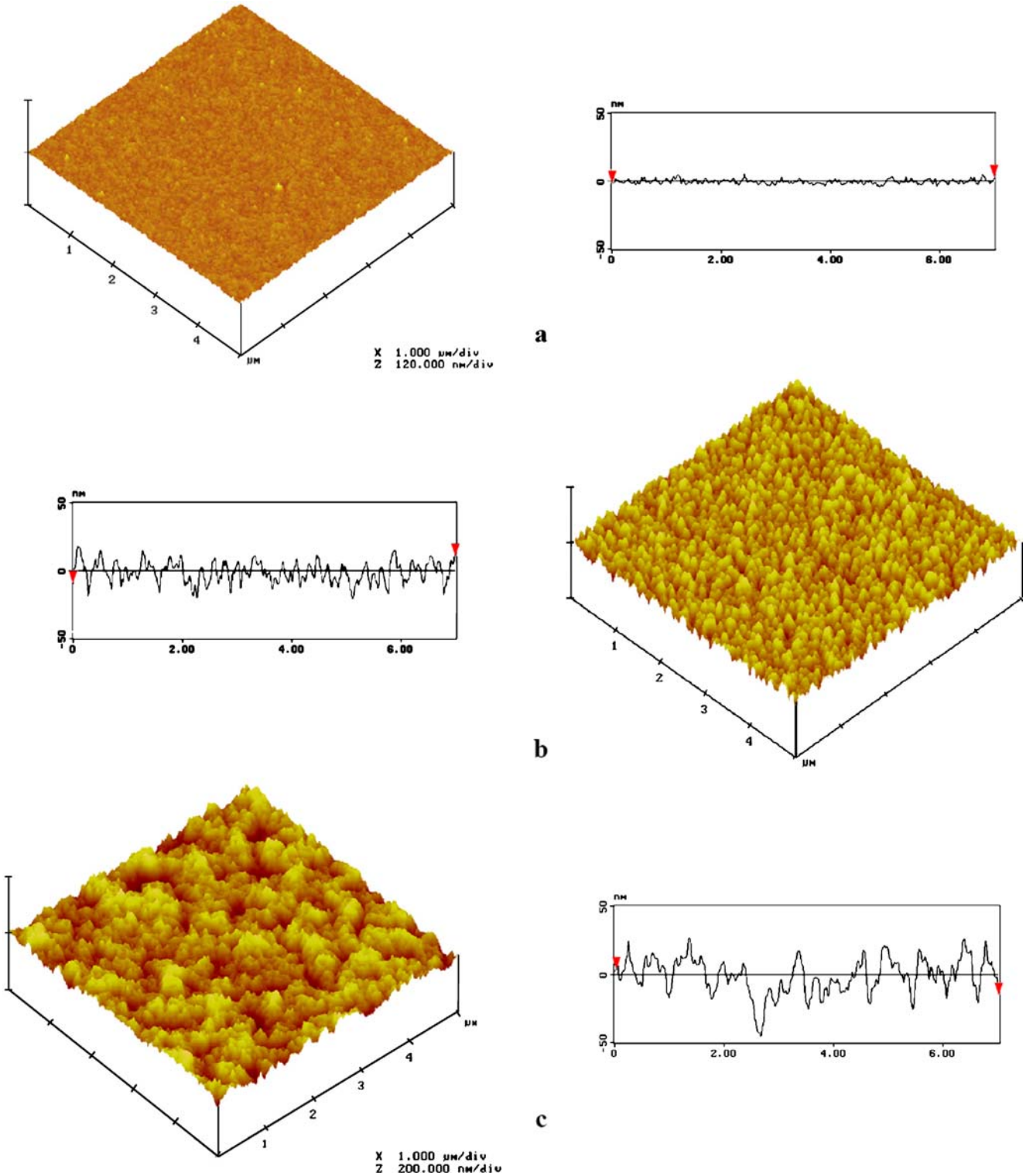

Fig. 10 Topographic images obtained by AFM (tapping mode) for Pty films grown with 10 (**a**), 25 (**b**), and 50 (**c**) potential cycles and corresponding profiles

increment in the film density involves a contribution of the solvent. The polymer volume fraction can be estimated as ranging from 0.63 to 0.20 in PTy films prepared with 25 to 50 potential cycles, respectively.

In fair agreement with the above-mentioned analysis is the information provided by the AFM imaging of the PTy modified electrodes, at different stages of polymer growth. As observable in Fig. 10, in all cases the Pt surface is fully covered by the polymer film; the thinnest film (Fig. 10a) exhibits a very smooth and regular morphology; as the number of polymerisation cycles increase, the polymer morphology becomes rougher, suggesting another route for polymer formation. Also, the remarkably regular topography (Fig. 10b) is not observed in films prepared with a higher number of potential cycles (Fig. 10c).

Aiming to find a consistent interpretation of the peculiar behaviour of Ty potentiodynamic polymerisation and of the whole set of results obtained in the present study (i.e. by the several employed methods, cyclic voltammetry, EQCM, ellipsometry and AFM), a tentative polymerisation mechanism, sketched in Fig. 11, has been considered. At least two different stages are involved in the process. In the first stage, one has the usual radical-cation formation and dimerisation, involving two electrons and the lost of two protons; the linear chain polymerisation gives rise to relatively short oligomers, poor or non-conducting, and thus the oxidation current decreases as the size of the oligomers increases and covers the electrode surface forming a smooth film. This new phase presents an increasing number of reactive sites (denoted by the stars), where new oligomeric chains can also be linked.

The late increase in the current is likely related to a second stage where the chain extension stops but the monomer oxidation continues and the polymerisation proceeds through those sites, justifying the observed polymer film rough morphology. Under this assumption, it is expected a non-linear but continuous increase in mass, in agreement with EQCM data; also, there will be an intermediate period, where the film deposition cannot be described by a homogeneous layer, which separates the two suggested polymerisation stages as supported by the ellipsometric information.

To provide support for the proposed mechanism for the Ty electrooxidation and polymerisation, ab initio calculations to predict the reactive sites in involved species have been carried out. In this theoretical study, the geometric

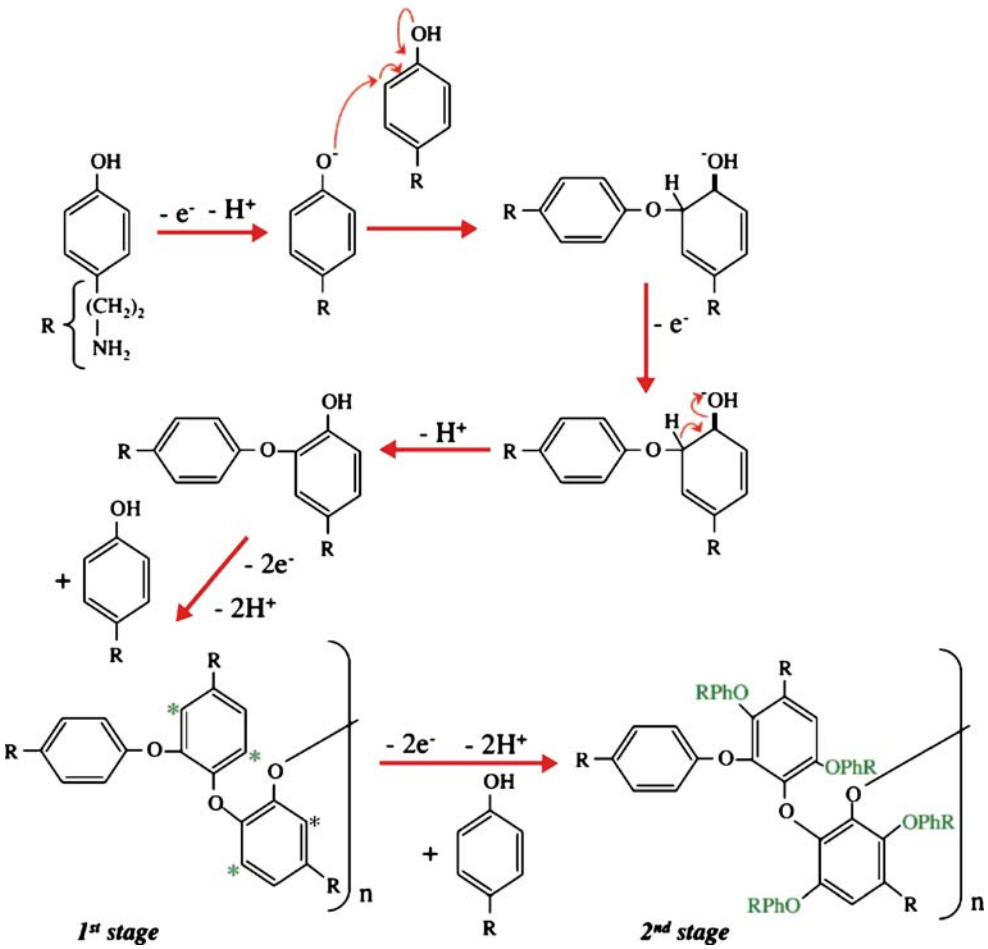

Fig. 11 Tentative mechanism for Ty polymerisation

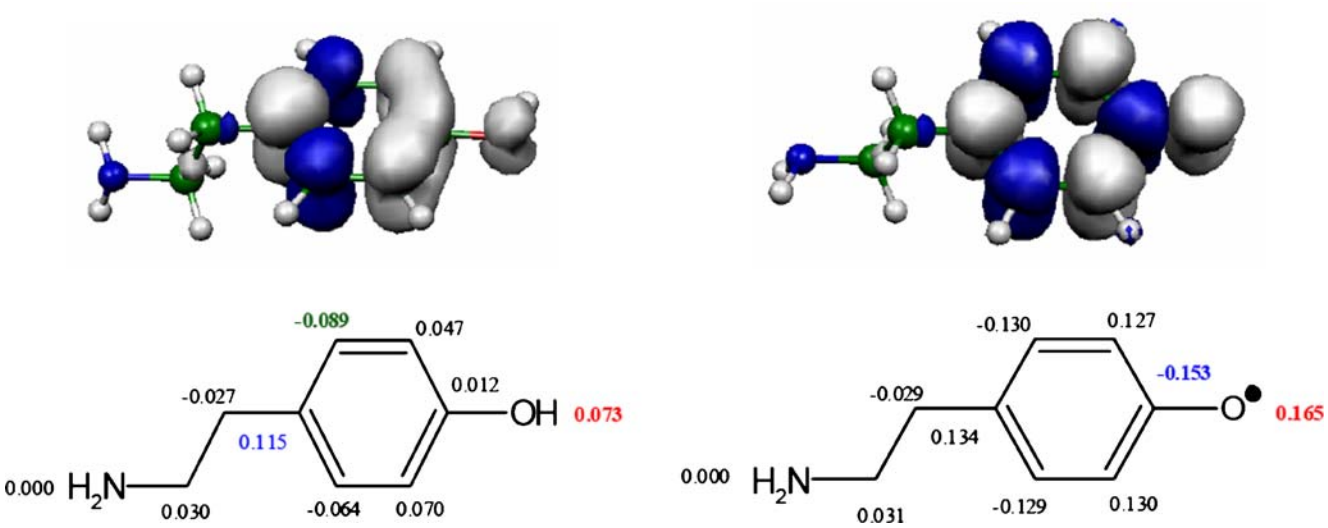

Fig. 12 Unpaired electron spin density distribution in neutral and cation radicals

structures assumed for the monomer, dimer and trimer, consider that the polymer film grows through the linkage of the O atom to the *ortho* position of the aromatic ring.

Two hypotheses have been explored for the radical generation: one involving the removal of an electron and a proton and the formation of a neutral radical and another considering the removal of an electron without proton lost and the generation of a radical cation.

The pictorial representation (Fig. 12) of spin distribution on the atoms demonstrates that there is a higher accumulation of spin at the O atom of the OH group and no delocalisation in the aromatic ring. A high local spin density

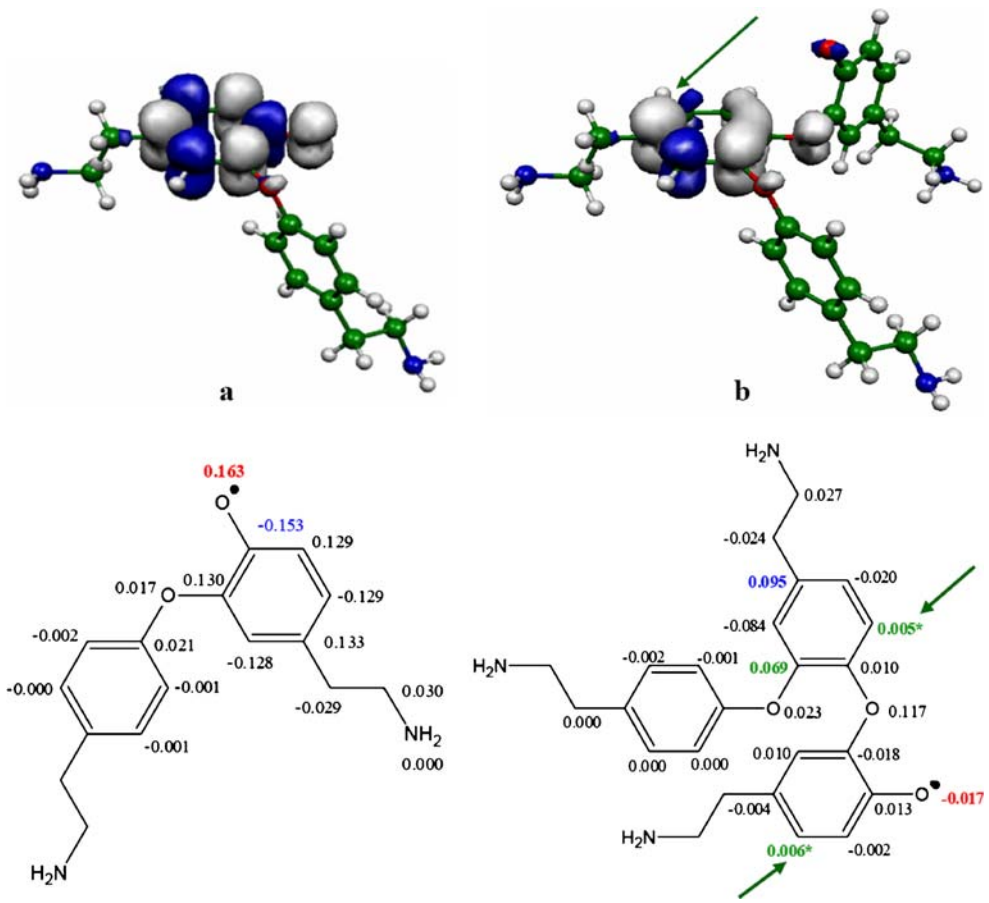

Fig. 13 Unpaired electron spin density distribution in dimer (**a**) and trimer (**b**)

is located at the *para*-position of the aromatic ring and on the O atom of the OH group. However, the linkage by the *para*-position is sterically hindered and such coupling would imply the removal of the amino side chain.

The neutral radical dimer presents similar features (Fig. 13a), whereas when a third unit is added to the dimer (Fig. 13b) there is some delocalisation of the spin in the aromatic ring of the second unit, suggesting that the coupling reaction should proceed by new reactive sites as indicated by the arrows.

Similar information was obtained for the monomeric radical cation. In both, monomer–radical and radical–radical coupling reactions, there is an increase of positive charge in the second and third units when a dimer and a trimmer are generated, respectively. This result predicts that the electron is removed from the monomer with –OH free groups, while the neutral radical or radical cation (of the monomer or dimer) that has suffered a nucleophilic attack of another monomer (or a recombination process during the coupling reaction) reestablishes its aromacity.

These ab initio calculations provide support to the previously described proposed mechanism, namely to the principal assumption on the increasing number of reactive sites when a new phase is formed in the electrode; obviously, thereafter a different polymerisation pathway should be considered and a faster deposition process expected, as the increase in mass (through EQCM) and in thickness (through ellipsometry) have demonstrated.

Conclusions

Coupled voltammetric and EQCM data have provided evidence that the potentiodynamic electrosynthesis of PTy in acidic media is not a self-limiting process and involves at least two regimens.

Ellipsometry has proven to be a powerful tool for the electropolymerisation process characterisation: the first stage of PTy growth is well described by the formation of a homogeneous isotropic film; over the first layer the growth is not uniform; thick PTy films present $\tilde{n}=1.454–0i$; the rate of polymer formation in each stage, is distinct.

As clearly revealed by AFM imaging, the morphology of PTy films is dependent on the number of potential scans: thin films present smooth surfaces, whereas thick layers are very rough.

A tentative electropolymerisation mechanism involving the deposition of a poor conducting layer by linear chain polymerisation followed by the formation of a non-planar polymer due to an increasing number of new reactive sites in the deposited material has been considered. Ab initio calculations provided support to the proposed mechanism: Ty electropolymerisation is initiated by the oxidation of the reactive O atom (–OH group); the monomer-radical coupling occurs by the *ortho* position resulting in dimer and trimer formation; the spin density distribution found for the trimer species rules out the possibility of the polymerisation process to proceed by the O atom; it continues through new coupling sites located in the aromatic ring.

Acknowledgments The authors acknowledge support from Fundação para a Ciência e Tecnologia (POCTI/ESP/39233/2001) and from CAPES and GRICES (Brasil-Portugal bilateral agreement, project 67/01).

The authors also wish to express their gratitude to Dr. Ana Viana for her kind help in obtaining the AFM images.

References

1. Yuqing M, Jianrong C, Xiaohua W (2004) Trends Biotechnol 22:227
2. Craig JD, O'Neill RD (2003) Anal Chim Acta 495:33
3. Ezerskis Z, Stalnionis G, Jusys Z (2002) J Appl Electrochem 32:49
4. Barbero C, Silber JJ, Sereno L (1989) J Electroanal Chem 263:333
5. Lapuente R, Cases F, Garcés P, Morallón, Vázquez JL (1998) J Electroanal Chem 451:163
6. Arslan G, Yazici B, Erbil M (2005) J Hazard Mater B124:37
7. Gattrell M, Kirk DW (1993) J Electrochem Soc 140:1534
8. Ezerskis Z, Jusys Z (2001) J Appl Electrochem 31:1117
9. Ferreira M, Varela H, Torresi RM, Tremiliosi-Filho G (2006) Electrochim Acta 52:434
10. Wang J, Jiang M, Lu F (1998) J Electroanal Chem 444:127
11. Gonçalves D, Faria RC, Yonashiro M, Bulhões LOS (2000) J Electroanal Chem 487:90
12. Dubois J-E, Lacaze P-C, Pham MC (1981) J Electroanal Chem 117:233
13. Tran LD, Piro B, Pham MC, Ledoan T, Angiari C, Dao LH, Teston F (2003) Synth Met 139:251
14. Sauerbrey GZ (1959) Z Phys 155:206
15. Frisch MJ, Trucks GW, Schlegel HB, Scuseria GE, Robb MA, Cheeseman JR, Zakrzewski VG, Montgomery JA Jr, Stratmann RE, Burant JC, Dapprich S, Millam JM, Daniels AD, Kudin KN, Strain MC, Farkas O, Tomasi J, Barone V, Cossi M, Cammi R, Mennucci B, Pomelli C, Adamo C, Clifford S, Ochterski J, Petersson GA, Ayala PY, Cui Q, Morokuma K, Malick DK, Rabuck AD, Raghavachari K, Foresman JB, Cioslowski J, Ortiz JV, Baboul AG, Stefanov BB, Liu G, Liashenko A, Piskorz P, Komaromi I, Gomperts R, Martin RL, Fox DJ, Keith T, Al-Laham MA, Peng CY, Nanayakkara A, Gonzalez C, Challacombe M, Gill PMW, Johnson B, Chen W, Wong MW, Andres JL, Gonzalez C, Head-Gordon M, Replogle ES, Pople JA. Gaussian 98, Revision A.7, x86-Linux-G98RevA.7Gaussian, Pittsburgh, PA, 1998.
16. Lüthi HP, Portmann S, Weber J. Molekel 4.3, Flükiger, Swiss Center for Scientific Computing Manno (Switzerland), 2000
17. Cordas CM, Tenreiro A, Abrantes LM (2003) EQCM study on the polytyramine modified electrodes for the preparation of biosensors. In: Gototsi YG, Uvarova IV (eds) Nanostructured materials and coatings for biomedical and sensor applications. Kluwer, pp 371–376
18. Tenreiro A, Cordas CM, Abrantes LM (2003) Portugaliae Electrochim Acta 21:361